NUMERICAL STUDY OF AN AEROSPIKE NOZZLE IN RETROPROPULSION

Ashish Vashishtha[1], Shashank Khurana[2], Dean Callaghan[3] & Cathal Nolan[1]

[1]Department of Aerospace and Mechanical Engineering, Institute of Technology Carlow, IRELAND.
[2]Department of Mechanical Engineering, BITS Pilani, Dubai Campus UAE.
[3]The Centre for Research & Enterprise in Engineering (engCORE), Institute of Technology Carlow, IRELAND.

Abstract

The primary motivation of this numerical study is to explore the feasibility of drag enhancement using aerospike nozzle for retropropulsion in hypersonic flow. An external expansion contoured aerospike nozzle with design Mach 3.0 have been attached to a $140°$ spherical cone re-entry body shape for retropropulsion. The two-dimensional axi-symmetric unsteady RANS numerical simulations are performed in freestream flow of hypersonic Mach number 7 using SU2 code. In order to compare the performance of the aerospike nozzle with circular and annular counter-flow jets, the exits of the annular nozzle and the circular nozzle have been modelled on the $140°$ spherical cone body as well. All three nozzles are simulated with mass flow condition equivalent to thrust coefficient 1. It was found that aerospike nozzle in retropropulsion provides a +28.4% drag enhancement (with respect to blunt nose without retropropulsion) due to it's contoured surface compared to +2.6% of annular and minute drag reduction for circular nozzle counter-flow jet.

Keywords: Numerical Simulation, Aerospike Nozzle, Retropropulsion, Hypersonic Flows, Deceleration

1. Introduction

Atmospheric entry to Earth or any other planet (e.g. Mars) requires a re-entry module to go through different phases of flow regimes from low-density flow to peak dynamic pressure and temperature regime in hypersonic flows to wake dominated supersonic and subsonic flows. Different techniques are developed for entry, descent and landing (EDL) of spacecraft depending on its trajectory, speed of entry, angle of entry and ballistic coefficient ($\beta = m/C_D A$). A lower ballistic coefficient is desirable for a quick deceleration and lower peak temperature during the hypersonic regime of EDL [1]. This can be achieved through different techniques such as a large area blunt nose [2, 3], hypersonic or supersonic inflatable aerodynamic decelerators (HIAD/SIAD) or parachutes of various geometries and configurations such as disk-band gap [1] and trailing ballutes[4]. Future manned and high payload missions with higher ballistic coefficients may not be able to use parachutes or HIAD / SIAD systems for deceleration because they may require high unrealistic high surface area for desired deceleration. The propulsive deceleration (retropropulsion) is another feasible technique, which can be utilized where aerodynamic deceleration may not be sufficient. Retropropulsion can be defined as placing a retrorocket in the opposite direction to the incoming flow field. Zang et al. [1] have reported challenges associated with future high β Mars missions and proposed eight architectures for EDL with various enabling technologies in aero-capture, hypersonic, supersonic and subsonic regimes. The propulsive deceleration is suggested in all subsonic landings and in half of supersonic deceleration, while one proposed architecture recommended propulsive deceleration all the way from entry, deceleration to landing. The simplicity in integrating retropropulsion coupled with the maturity level in propulsion technology, makes it one of the attractive techniques for EDL. However, the interaction of rocket plumes with freestream hypersonic or supersonic regimes can be highly complex and can

Table 1 – Freestream Conditions

Property	Specification
Mach Number (M_∞)	7.0
Stagnation Temperature ($T_{\infty,0}$)	600 K
Freestream Pressure (P_∞)	229.47 Pa
Freestream Temperature (T_∞)	55.55 K
Freestream Speed (V_∞)	1045.94 m/s
Freestream Density (ρ_∞)	0.0143892 kg/m^3
Unit Reynolds Number	4.7×10^4 /cm

lead to reduced aerodynamic deceleration. The disturbance or pushing back of the bow shock at the stagnation region due to interaction of counter-flow jet and the creation of low pressure re-circulation regions on the outskirts of a blunt body can lead to an overall reduction in aerodynamic drag levels. The circular nozzle at the center of a blunt body has been studied extensively for drag and aerodynamic heating reduction at hypersonic and high supersonic flows [5], mainly with air. In a very few studies, Vashishtha et al. [6] and Peter et al.[7] have investigated direct reactive and light gas injection in stagnation zone of blunt nose. However, the configuration of different peripheral counterflow jet have been found to preserve and slightly augment the aerodynamic drag in supersonic [8] or hypersonic flows [9]. The circular supersonic nozzle with fixed exit area can be operated optimally at the design altitude and the exit jet may behave overexpanded or underexpanded based on pressure at different altitude. The working principle and flow field of different altitude adaptive advanced nozzles have been discussed by Sutton [10] and Hagemann et al. [11]. The premise of the current study is that it may be better to use altitude adaptive advanced nozzle during the all propulsive EDL phases, with a single nozzle capable of working at all the altitudes. Among the various configurations discussed by Hagemann [11], the aerospike nozzle can be considered a good candidate for retropropulsion in hypersonic flows as well as low-altitude supersonic and subsonic flows. It is expected that aerospike nozzle can contribute to a higher drag coefficient due to it's contoured spike surface. Danielson [12] studied the aerospike nozzle (with thrust coefficient, C_T = 2 and 4.0) as retropropulsion in supersonic flow and did not find any aerodynamic drag enhancement apart from favourable thrust provided by nozzle. In general, the drag augmentation in retropropulsion or drag reduction using counter-flow jets depends highly on how the exit jet and incoming flow interact with each other as well as with the vehicle body. The performance of counter-flow jet or supersonic retropropulsion have been characterized in various studies over a range of operating parameters, such as: 1) Jet to freestream momentum ratio (R_M) [13], 2) Jet to freestream total pressure ratio (R_P) [9] and 3) Thrust coefficient (C_T) [14]. All three parameters represent the ratio of jet to incoming flow strength with slight variation in formulation. Apart from the operating parameters, the location and size of central or peripheral nozzles with respect to blunt body diameter also influence drag augmentation or reduction. Overall there are several different parameters involved in performance assessment of retropropulsion in hypersonic or supersonic regimes. This study is motivated to understand the integration of aerospike nozzle to re-entry shapes. The performance and flow interaction of three equivalent nozzles circular, annular and aerospike nozzles are numerically studied for same thrust coefficient $C_T = 1.0$. The objectives of the study are defined as: 1) Develop an understanding of the the flow-field interaction between the incoming hypersonic flow and the aerospike nozzle jet, 2) Compare the performance of the aerospike nozzle with equivalent annular and circular nozzles at $C_T =1.0$.

2. Numerical Method

The 2D axi-symmetric unsteady compressible Reynolds Averaged Navier Stokes Equations, with two-equation $k - \omega$ SST Turbulence Model, have been solved using the Stanford University Unstructured (SU^2) solver [15]. Figure 1a shows the computational domain for an aerospike nozzle attached to a $140°$ conical blunt nose. A single zone structured mesh (151×151) has been used for $140°$ spherical cone with no jet or central and annular nozzle counter-flow jets as shown in Fig. 1b. The external

(a) Computational Domain for Aerospike

(b) Single Zone Mesh for Blunt Nose

(c) Multizone Mesh for Aerospike Nozzle
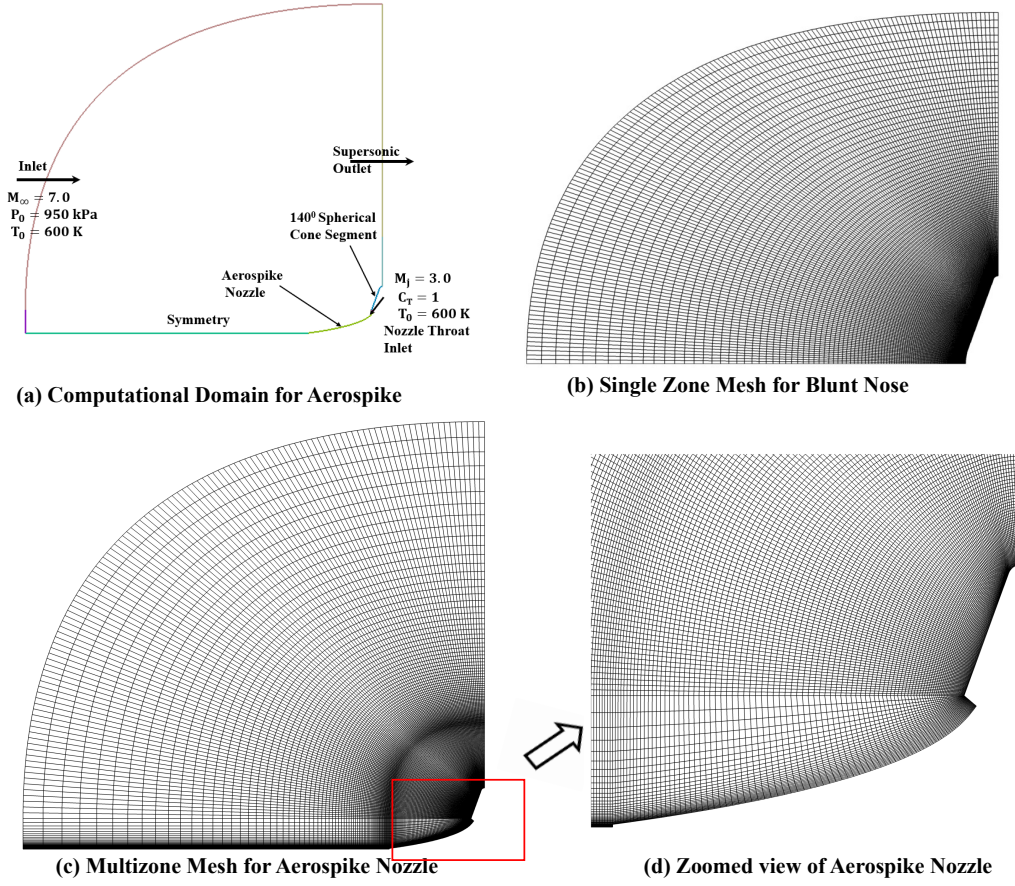

(d) Zoomed view of Aerospike Nozzle

Figure 1 – (a) Computational Domain for Aerospike Nozzle attach to $140°$ blunt cone, (b) Single Zone grid for No jet, central jet ON and annular jet ON cases, (c) Multi-zone grid for Aerospike Nozzle with blunt cone (d) Zoomed View of Aerospike Nozzle

expansion contoured aerospike (EE Aerospike) nozzle of exit Mach number (M_j = 3) have been de-signed based on the characteristic lines of supersonic expansion through nozzle contour [16]. The aerospike nozzle is attached to the $140°$ spherical cone, and a multi-zone structured mesh has been generated as shown in Fig. 1c and 1d. The inlet boundary condition is defined as freestream hy-personic Mach 7 conditions of the Kashiwa Hypersonic Wind Tunnel test-section [17] with stagnation pressure and temperature as 950kPa and 600K, respectively. The freestream conditions are shown in Table 1. The retro-nozzle conditions are modelled based on $C_T = 1$ for all the three nozzles, which are shown in Table 2. The thrust from any retro nozzle can be modelled as follows:

$$T = (P_e - P_a)A_e sin(\delta) + \rho_e V_e^2 A_e sin(\delta) = P_e A_e sin(\delta)(1 + \gamma_e M_e^2) \quad (1)$$

$$C_T = \frac{2T}{\gamma_\infty M_\infty^2 P_\infty A_\infty} \quad (2)$$

$$C_T = \frac{2(1 + \gamma_e M_e^2)sin(\delta)}{\gamma_\infty M_\infty^2} \frac{P_e}{P_\infty} \frac{A_e}{A_\infty} \quad (3)$$

where, subscript (e) and (∞) are exit and freestream parameters, respectively. The δ is the angle of flow turning from the nozzle exit plane with respect to freestream direction. In case of circular and annular nozzle, the exit of nozzle plane is perpendicular to freestream, hence δ is zero. In case of aerospike nozzle, the δ is by design Prandtl-Meyer turning angle. The circular nozzle exit diameter was considered as $d_j = 0.2D_m$ and the gap for annular nozzle was kept as $0.1D_m$, while inner and outer diameters $D_i = 0.15D_m$, $D_o = 0.25D_m$, respectively. In case of annular nozzle, the exit area is higher than central nozzle exit area, even through same exit dimension. To generate same thrust ($C_T = 1.0$) from both the nozzles, the pressure boundary condition for nozzle exit was adjusted in both the cases, while exit velocity and temperature will remain the same.

Table 2 – Throat and Nozzle Exit Conditions for counter-jet nozzle

Property	Specification
Design Mach Number (M_j)	3.0
Stagnation Temperature ($T_{j,0}$)	600 K
Exit Temperature (T_j)	214.28 K
Exit Speed (V_j)	880 m/s
Throat Temperature (T^*)	500.0 K
Throat Speed (V^*)	448.22 m/s

In aerospike nozzle, the supersonic jet is expanded externally, with one side fluid boundary and other side curved wall boundary. The supersonic flow is accelerated through Prandtl-Meyer Expansions. The curved sections of aerospike nozzle can be designed based on desired expansion regions either internal/external expansion (IE aerospike) or only external expansion (EE aerospike). These two designs are different as the throat (minimum area) region is at the lip in case of EE aerospike nozzle and expansion only occur externally. However, in case of IE aerospike nozzle, the throat is inside the annular region and acceleration of flow occur internally as well as externally [16]. Due to simplicity of modelling EE aerospike nozzle is integrated to $140°$ blunt cone as shown in Fig. 1a. The shroud lip is kept on the blunt nose at location $y = 0.25D_m$. The boundary condition at inlet of aerospike nozzle was considered as throat condition according to $C_T = 1.0$. However, the exit dimension of EE aerospike nozzle throat is governed by flow turning requirement due to design Mach number as well as outer annular lip location. Hence, the exit dimension are different than annular nozzle and central nozzle used. The inlet velocity applied is perpendicular to the throat surface, which leads to higher mass flow rate requirement to achieve same $C_T = 1.0$, where thrust is computed only because of momentum thrust and pressure thrust at the nozzle exit.

The flow-fields have been initialized with freestream conditions. The unsteady numerical solver uses the second order accurate dual time-stepping method along with AUSM+UP2 scheme for inviscid term and average of gradient for viscous terms. Air has been treated as an ideal gas. The supersonic outlet has been used as an outlet boundary condition and the symmetry boundary condition is used for the centerline axis. A small step near the end of aerospike nozzle has been used to avoid inaccurate computation of the source term in 2D axisymmetric RANS equation at the junction of wall and symmetry boundary. In this study, three different cases of $C_T = 1.0$ have been simulated for 5 ms time duration with 15 inner iteration in implicit time solver along with single case of no jet injection.

3. Results & Discussions

The simulation results are obtained by 2D axisymmetric unsteady compressible RANS solver with $k - \omega$ SST turbulence model. The shock waves in front of blunt nose as well as blunt nose with counterjet are stabilized by 5 ms simulation time. The results obtained at final time are analysed through computed drag coefficient, obtained Mach contours and pressure plots on blunt nose as well as comment on performance of aerospike nozzle.

Table 3 – Computed Total Axial Force Coefficient $C_A = C_D + C_T$

S.No.	Case	Components	Total (C_A)
1.	No Jet	$C_D = 1.267$, $C_T = 0$	1.267
2.	Circular Nozzle	$C_D = 0.259$, $C_T = 1.0$	1.259
3.	Annular Nozzle	$C_D = 0.300$, $C_T = 1.0$	1.300
4.	Aerospike Nozzle	Blunt Nose: $C_D = 0.076$,	
		Spike Region: $C_D = 0.551$,	
		$C_T = 1.0$	1.627

Table 3 shows the computed total drag coefficient as well its components. After stabilizing the flow field with in 5 ms of simulations time, the computed drag coefficients does not change with time. The blunt nose experiences drag coefficient as 1.267, while there is no counter-flow jet ($C_T = 0.0$). The

rest of computation assumes thrust coefficient for all three cases as $C_T = 1.0$. The computed drag coefficients are added to assumed C_T values to obtain total axial force coefficient. The computed drag coefficient at blunt nose for integrated circular nozzle counter-flow jet is 0.259, which leads to total axial force coefficient as 1.259, lower than blunt nose without counter-jet. The annular nozzle integrated with $140°$ blunt nose, with same exit mass flow rate as circular nozzle and $C_T = 1$ condition, shows slight higher drag coefficient on the blunt nose, causing total axial force higher than the circular nozzle counter-jet as well as higher than no jet (only blunt nose) case. In case of aerospike nozzle operating at $C_T = 1.0$, the blunt nose skirt region, experiences least drag and major drag comes from the high pressure on the spike wall, such that the total axial force coefficient becomes 1.627, a total 28.4 % increase in comparison to the drag on blunt nose without any counter-jet. These comparison between drag coefficient shows effectiveness of aerospike nozzle for a given condition as drag enhancing device during retroproplusion. However, the air exits from the throat of EE aerospike nozzle at P-M expansion angle, which causes the increase in mass flow rate to produce the thrust equivalent to $C_T = 1.0$ at lower throat velocity, in comparison to straight counter-jet exited from circular or annular nozzle. Hence, it may be required to compare the performance of aerospike nozzle, not only for same $C_T = 1.0$, but also other performance parameters such as mass flow rate, same stagnation pressure ratio etc in future studies. It may be further interesting to study the effect of internal external expansion aerospike nozzle (IE aerospike) in retropropulsion at different altitude conditions. In next subsections, Mach contour, flow field variation has been compared to understand the drag enhancement by aerospike nozzle.
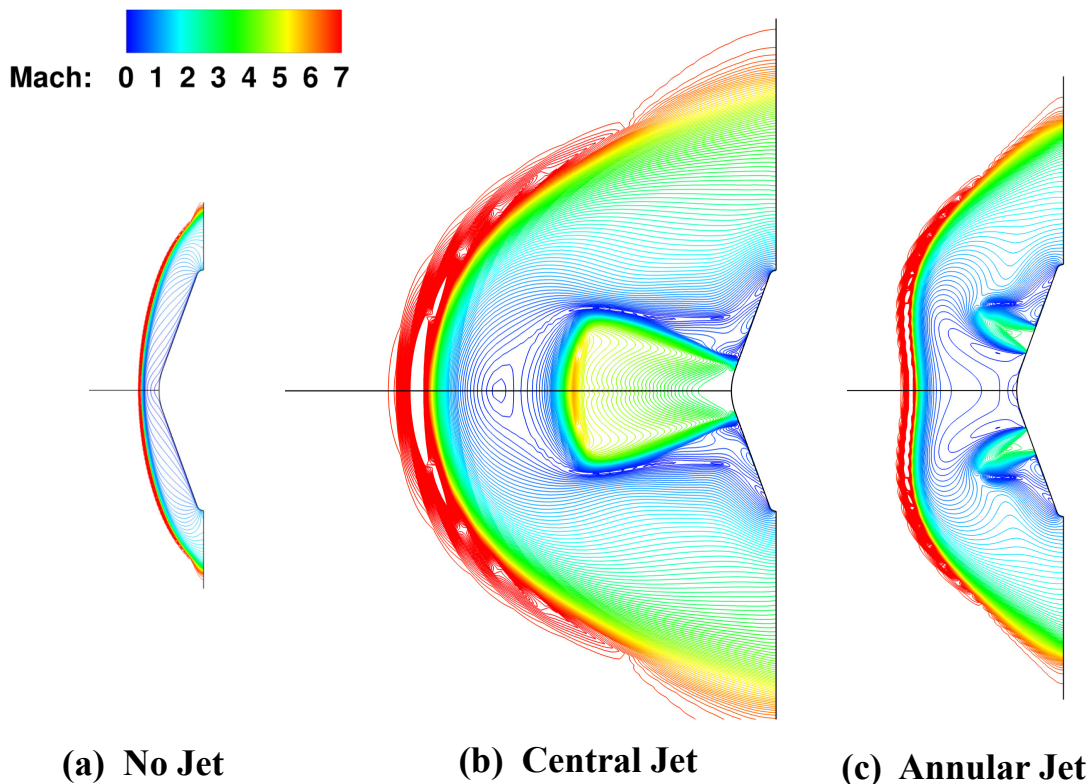

(a) No Jet   **(b) Central Jet**   **(c) Annular Jet**

Figure 2 – Mach Contours for (a) $140°$ Spherical Nose blunt cone without any jet, (b) central nozzle counter jet, (c) annular nozzle counter jet

Figure 2 shows the Mach contours for three cases blunt nose without any counter-flow jet, the counter-jet from central nozzle as well as counter-flow jet from annular nozzle. In case of no counter-flow jet, the bow shock at hypersonic Mach number 7, established itself in front of blunt nose close to the body and high pressure compressed air region between the bow-shock the blunt nose causes maximum drag as mentioned in previous table. The second case of counter-flow jet from the central nozzle pushes the the frontal bow shock at the maximum distance from the highly underexpanded jet coming out from the nozzle. The flow features exhibits the typical flow structure formed at short

penetration mode of counter-flow jet [18], the stagnation region between frontal bow shock and the jet shock. The re-circulation region formed near the root of jet exit at the blunt nose caused low drag on the blunt nose region. As the jet is highly underexpanded, the envelop of frontal shock wave expands in larger region, the re-attachment point frontal shock does not exist. The lower total axial force is caused by low pressure region on the blunt nose region. In case of counter-flow jet from annular nozzle, the bow shock is manipulated near the side regions as shown in Fig. 2c. The bow shock manipulation only in the side region, doesn't reduce to overall axial force coefficient for the annular counter-flow jet significantly. The total axial force coefficient is slightly higher than the circular counter-flow jet. The overall envelop of frontal shock wave increases in lateral direction similar to circular nozzle, however, the central region of bow shock is closer to the body in comparison to circular counter-flow jet.
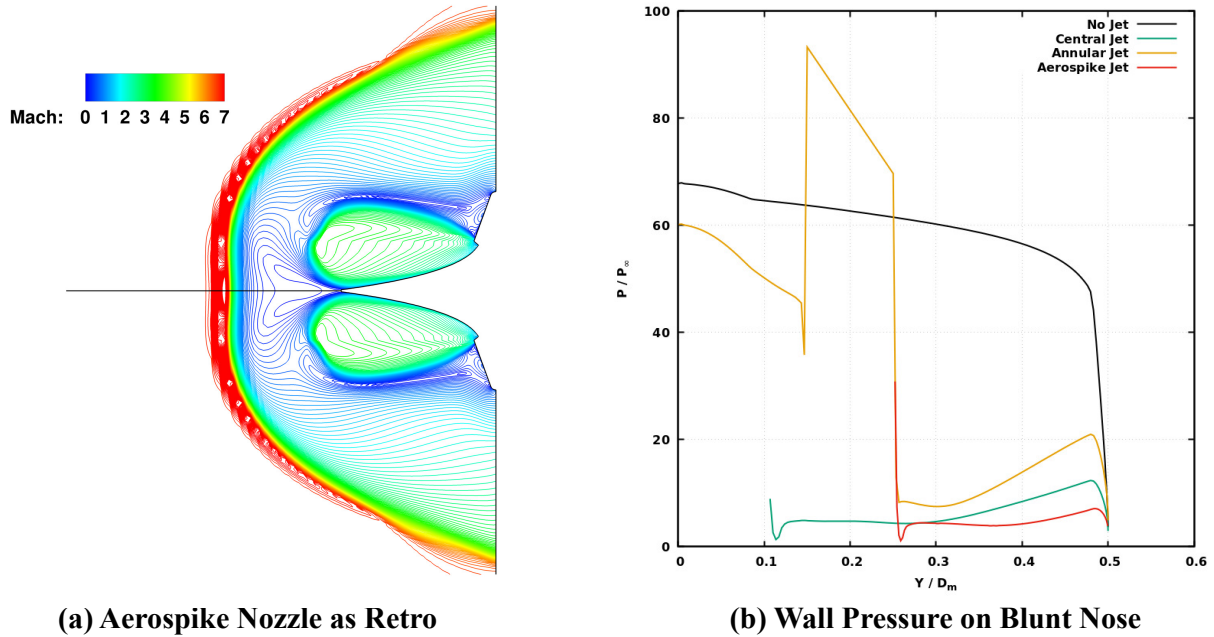

(a) Aerospike Nozzle as Retro

(b) Wall Pressure on Blunt Nose

Figure 3 – Mach Contours for (a) $140°$ Spherical Nose blunt cone with (a) aerospike counter jet nozzle (b) Wall Pressure for three counter-flow jet cases

Figure 3a shows the Mach contours for integrated aerospike nozzle with the $140°$ cone. As the operating condition suggest highly underexpanded jet. The lateral envelop of frontal bow shock, increases with all the counter-flow jet. The counter-flow jet coming out from the throat exit, expands to higher speeds, bounded with the spike wall as well as free shear flow. The blunt nose region is remains in low-pressure region, causes highest drop in drag only on the blunt nose region in comparison to circular or annular nozzle. The spike region of aerospike nozzle experiences the high pressure on the spike wall. The high drag contribution of spike wall leads to higher overall axial force coefficient in comparison to other nozzles. As aerospike nozzle performs well as altitudes compensating nozzle, its effectiveness for retropropulsion may be investigated in future study for range of overexpanded and underexpanded jet exits. Fig. 3b shows the wall pressure curve for blunt nose by plotting non-dimensional pressure (P/P_∞). The no-jet case shows the typical wall pressure variation as almost constant up to the corner of blunt nose due to extent of stagnation zone, further drop in wall pressure due of expansion at the corner. the central counter-flow jet causes the wall pressure on the blunt nose drops significantly, remains almost constant for the extent of blunt nose, except near the corner. The wall pressure curve for annular counter-jet exhibits higher wall pressure near the central region of blunt nose (still lower than the no-jet case). However, the wall pressure at the skirt of blunt nose drops below the central region wall pressure, due to interaction of annular jet. The wall pressure at the blunt nose skirt is still higher than typical central-jet as well as aerospike jet. In case of counter-flow jet from aerospike nozzle, the re-circulation region at the root of exiting jet, the lowest wall pressure is observed on the skirt of blunt nose. The major contribution in high axial force coefficient comes from high pressure on the spike region. As mentioned earlier that this

study compares the performace of different counter-flow jet nozzles only one specific freestream and operating conditions, which shows effectiveness of aerospike nozzle as retropropulsion and expected to perform at all the altitudes. It is further required to investigation the performance of aerospike nozzle at various altitude by numerical or experimental studies.

4. Conclusions

In this study, preliminary investigation of integration of aerospike nozzle to blunt nose body and its performance as retropropulsion device on a particular hypersonic Mach number with specific nozzle operation is completed. The unsteady 2D axi-symmetric compressible Navier-Stokes equations have been solved with RANS turbulence modelling using SU^2 solver for supersonic counter-flow jet flow from designed nozzles at Mach 3.0 in freestream hypersonic flow of Mach 7. The aerospike nozzle exhibits its effectiveness for retropropulsion such as it increases the overall axial force coefficient by 28.4% in comparison to drag coefficient of blunt nose without counter-flow jet. In this study only a single performance parameter $C_T = 1.0$ is compared for all three very different nozzles for retropropulsion application and aerospike nozzle is found to be effective, even in the studied highly underexpanded case. In the future study, it is recommended to throughly investigate the performance of aerospike nozzle not only agains various operating parameters such as mass flow rate from the nozzle, operating stagnation pressure ratio etc, but also at different altitude and range of incoming freestream Mach numbers.

Contact Author Email Address

mail to: ashish.vashishtha@itcarlow.ie

Copyright Statement

Acknowledgments

References

[1] Zang T, Cianciolo A D, Kinney D, Howard A, Chen G, Ivanov M, Sostaric R, and Westhelle C. Overview of the nasa entry, descent and landing systems analysis study. In *AIAA SPACE 2010 Conference & Exposition*, pages 1–11. AIAA 2010-8649, 2010. doi: 10.2514/6.2010-8649.

[2] Yamada K, Akita D, Sato E, Suzuki K, Narumi T, and Abe T. Flare-type membrane aeroshell flight test at free drop from a balloon. *Journal of Spacecraft and Rockets*, 46(3):606–614, 2009. doi: 10.2514/1.40912.

[3] Watanabe Y, Suzuki K, Imamura O, and Yamada K. Attitude estimation of nano-satellite with deployable aeroshell during orbital decay. *Transaction of the Japan Society for Aeronautical and Space Sciences, Aerospace Technology Japan*, 14(ists30):Pf_1–Pf_5, 2016. doi: 10.2322/tastj.14.Pf_1.

[4] Chaubdar P, Harichandan A B, Vashishtha A, and Jagadeesh G. Experimental and numerical studies of toroidal ballute in hypersonic shock tunnel. In 6th *National Symposium of Shock Wave*, 2020. URL https://www.researchgate.net/publication/339552027.

[5] Mahmoud YM Ahmed and Qin N. Forebody shock control devices for drag and aero-heating reduction: A comprehensive survey with a practical perspective. *Progress in Aerospace Sciences*, 112:100585, 2020. ISSN 0376-0421. doi: 10.1016/j.paerosci.2019.100585.

[6] Vashishtha A, Callaghan D, and Nolan C. Drag control by hydrogen injection in shocked stagnation zone of blunt nose. *IOP Conference Series: Materials Science and Engineering*, 1024(1):012110, jan 2021. doi: 10.1088/1757-899x/1024/1/012110.

[7] Harmon P, Vashishtha A, Callaghan D, Nolan C, and Deiterding R. Study of direct gas injection into stagnation zone of blunt nose at hypersonic flow. In *AIAA Propulsion & Energy Forum*. AIAA 2021-3529, 2021. doi: 10.2514/6.2021-3529.

[8] Bakhtian N M and Aftosmis M J. Parametric study of peripheral nozzle configurations for supersonic retropropulsion. *Journal of Spacecraft and Rockets*, 47(6):935–950, 2010. doi: 10.2514/1.48887.

[9] Keyes J W and Hefner J N. Effect of forward-facing jets on aerodynamic characteristics of blunt configurations at mach 6. *Journal of Spacecraft and Rockets*, 4(4):533–534, 1967. doi: 10.2514/3.28900.

[10] G.P. Sutton and O. Biblarz. *Rocket Propulsion Elements*. Wiley, 2016. ISBN 9781118753880. URL `https://books.google.ie/books?id=2qehDQAAQBAJ`.

[11] Hagemann G, Immich H, Van Nguyen T, and Dumnov G E. Advanced rocket nozzles. *Journal of Propulsion and Power*, 14(5):620–634, 1998. doi: 10.2514/2.5354.

[12] Danielson T. Vehicle integrated aerospike for high mass mars missions. Master's thesis, Purdue University, Purdue USA, 2017. URL `https://docs.lib.purdue.edu/dissertations/AAI10684728/`.

[13] Desai S, Prakash K V, Kulkarni V, and Gadgil H. Universal scaling parameter for a counter jet drag reduction technique in supersonic flows. *Physics of Fluids*, 32(3):036105, 2020. doi: 10.1063/1.5140029.

[14] Jarvinen P O and Adams R H. *The aerodynamic characteristics of large angled cones with retrorockets*. NASA-CR-12472. Unclassified NASA Technical Report, 1970. URL `https://ntrs.nasa.gov/archive/nasa/casi.ntrs.nasa.gov/19720005324.pdf`.

[15] Economon T D, Palacios F, Copeland S R, Lukaczyk T W, and Alonso J J. Su2: An open-source suite for multiphysics simulation and design. *AIAA Journal*, 54(3):828–846, 2016. doi: 10.2514/1.J053813.

[16] Denton B L. Design and analysis of rocket nozzle contours for launching pico-satellites. Master's thesis, RIT Main Campus, 2008. URL `https://scholarworks.rit.edu/theses/5818`.

[17] Vashishtha A. *Bow-Shock Instability and its Control in front of Concave shaped Blunt Nose at Hypersonic Mach No. 7*. Ph.d. thesis, The University of Tokyo, 2016. Thesis Number: 12601 A No. 33230.

[18] Shang J. S., Hayes J., Wurtzler K., and Strang W. Jet-spike bifurcation in high-speed flows. *AIAA Journal*, 39(6):1159–1165, 2001. doi: 10.2514/2.1430.